J Nondestruct Eval (2016) 35:8
DOI 10.1007/s10921-015-0325-5

Remote Real Time Monitoring for Underground Contamination in Mongolia Using Electrical Impedance Tomography

Munkh-Erdene Ts[1] · Eunjung Lee[2] · Liangdong Zhou[2] · Kyoung Hun Lee[2] · Jin Keun Seo[2]

Received: 10 April 2015 / Accepted: 7 December 2015 / Published online: 15 December 2015

Abstract Mongolia's abundant natural resources have driven much recent economic development and with it the need for an underground contamination monitoring system. For instance, the fast growth of the mining industry coincides with underground contamination caused by petrol, copper tailings, mercury, etc. These contaminants are highly electrically conductive, and can therefore be assessed by electrical impedance tomography (EIT). This non-destructive and inexpensive method can visualize the conductivity distribution of a target area, and is suited for use in Mongolia. A number of electrodes are placed on the ground surface to induce currents and to measure the resulting voltages. We introduce a new electrode configuration, and use the local projective conductivity image method to monitor the near-surface area. Additionally, conventional EIT is used to monitor areas deeper underground. The collected voltage data can be used for both algorithms–separate measurements are not required–allowing near real-time monitoring for underground contamination.

✉ Eunjung Lee
eunjunglee@yonsei.ac.kr

Munkh-Erdene Ts
ts.munkherdene@must.edu.mn

Liangdong Zhou
zhould1990@hotmail.com

Kyoung Hun Lee
imlkh@yonsei.ac.kr

Jin Keun Seo
seoj@yonsei.ac.kr

[1] School of Applied Science, Mongolian University of Science and Technology, Ulaanbaatar, Mongolia

[2] Department of Computational Science and Engineering, Yonsei University, 50 Yonsei-ro, Seodaemun-gu, Seoul 120-749, South Korea

Keywords Underground contamination · Electrical impedance tomography · Long-term remote monitoring

Mathematics Subject Classification 65Z99

1 Introduction

Mongolia has the characteristic of a large land area accompanied by a very low population density. The country's natural resources, and thus mining, have high economic importance. The Mongolian government estimates there to be about thirty thousand informal gold miners, but an independent survey suggests that at least a hundred thousand miners are working in the country for all companies, from large to artisanal [8]. The extraction and processing of ores generally require the use of harmful chemicals. In 2008, the UN reported that the entire population, around two thousand, of a rural village named "Khongor Soum", located north of the capital city Ulaanbaatar, had excessive mercury levels due to pollution, and that animals and livestock in the area were also affected [10]. The costly operation of neutralizing polluted soil and revivifying the environment of this area is ongoing. The desire to prevent these costs is driving a demand for monitoring systems suitable for use in Mongolia.

Because of the country's extensive size and the sparse population in areas of suspected contamination, a low-cost remote monitoring system is required. In addition, detecting and monitoring underground contamination pose the challenge of locating contaminants only by observing the surface (without excavation), and by the fact that the situation is already serious by the time contaminants reach the surface. This paper proposes a remote near-real-time method for monitoring underground contamination that uses electrical impedance tomography (EIT), which is non-destructive, non-

invasive, cheap to maintain, and requires little manpower. EIT uses the relation between electrical current and voltage to compile tomographic images [1,2,7,15], by determining the electrical impedance inside an electrically conducting object from knowledge of the injected current and the measured voltage data. The generally static nature of the ground allows the continuous monitoring of changes in underground conductivity distribution to reveal any emerging variations in underground contamination. Typically, a target area with a high conductivity contrast is advantageous for monitoring by EIT. Moreover, monitoring geoelectrical properties by EIT can provide results in near-real-time, or on demand. The recorded data can then be transmitted via several communication methods to a distant location.

Various works have used electrical impedance and resistance tomography in the detection and monitoring of land contamination; see [4,5,9,13,16] and references therein. Most previous methods using EIT employed electrodes/sensors on the ground surface as well as in boreholes deep enough to guarantee good measurement data.

Common mining contaminants are highly conductive, as are heavy industrial contaminants such as benzene, toluene, xylenes, tetrachloroethene, and trichloroethene [3,14]. In this paper, we propose a new electrode configuration to monitor the conductivity distribution of a target region, using conventional EIT and the local projective image method [12], which each have advantages for use in different sub-surface areas. Unlike in other approaches, the current-injecting and data-collecting electrodes are arranged uniquely and placed on the ground surface only. Conventional EIT supplies a low-resolution three-dimensional reconstructed conductivity distributional image for the deep underground area, and the local projective conductivity image method provides a high-resolution image of the near-surface area. Gathering data by both methods provides information about the geoelectrical properties of both shallow and deeper areas below the surface.

2 Underground Contamination Monitoring Using EIT Techniques

To monitor underground contamination of a suspected area using EIT, an array of electrodes is placed on the ground surface to collect the voltage data and to observe the changes with time of the conductivity distribution beneath the surface.

2.1 Electrode Configuration

On the ground surface, we place an array of $(M \times N + 1)^2$ number of electrodes uniformly with 1 m intervals, as shown in Fig. 1b. For ease of explanation, we assume that the array has electrodes at points (i, j) for $i, j = 0, 1, \ldots, M \times N$. The electrodes at positions (iN, jN), $i, j = 0, 1, \ldots, M$ are capable of both driving and sensing so that $(M+1)^2 - 1$ linearly independent currents are injected, as in a conventional EIT system. The other electrodes are for sensing only, to collect the boundary voltages at each sampling time t. Note that $M, N = 4$ in Fig. 1.

The injection of a current of I mA using a chosen pair of electrodes at positions P^+ and P^- results in a potential $u(\mathbf{r}, t)$ that satisfies

$$\nabla \cdot (\sigma(\mathbf{r}, t)\nabla u(\mathbf{r}, t)) = 0 \tag{1}$$

with boundary condition

$$\sigma(\mathbf{r}, t)\frac{\partial u(\mathbf{r}, t)}{\partial \mathbf{n}} = I\left(\delta(\mathbf{r} - P^+) - \delta(\mathbf{r} - P^-)\right),$$

where $\sigma(\mathbf{r}, t)$ is the conductivity at time t and position $\mathbf{r} = (x, y, z)$, $\mathbf{n}$ is the unit vector normal to and outward from the boundary, and $\delta(\mathbf{r})$ is the Dirac delta function. Here, electrodes are considered as points, because they are very small compared with the size of the surface.

Denoting the boundary voltage at time t and position (i, j) by $V_{\mathrm{i,j}}(t) = u((i, j, z_{\mathrm{ground}}), t)$, we collect the data vector

$$\mathbf{V}(t) = (V_{0,0}(t), V_{0,\mathrm{N}}(t), \ldots, V_{\mathrm{MN,MN}}(t)).$$

These voltage data are measured for each $(M+1)^2 - 1$ linearly independent current to visualize the time changes of conductivity distribution. In practice, the voltage data measured on each current-carrying electrode are excluded to avoid the contact impedance problem. Moreover, the use of difference data in the methods proposed here averts the influences of contact impedance as well as singularities caused by point electrodes [6].

2.2 Local Projective Conductivity Image

Conventional EIT reconstruction using the driving and sensing electrodes at positions (iN, jN) can provide time-varying conductivity images. It uses linearization to construct a sensitivity matrix based on the relation between the boundary potential difference and the conductivity perturbation in the interior of the domain. The ill-posedness of the resulting EIT problem gives low spatial resolution [2,11]. Therefore, we employ an additional imaging technique, called the local projective conductivity image method, using supplementary sensing-only electrodes [12].

For an overview of the proposed method, let us explain how to produce the projective image on the local surface $[1, 2N-1] \times [1, 2N-1]$, as in Fig. 2. In fact, a local surface $[1, kN-1] \times [1, kN-1]$ for any positive integer k can be used depending on the target coverage. Using the linearity between

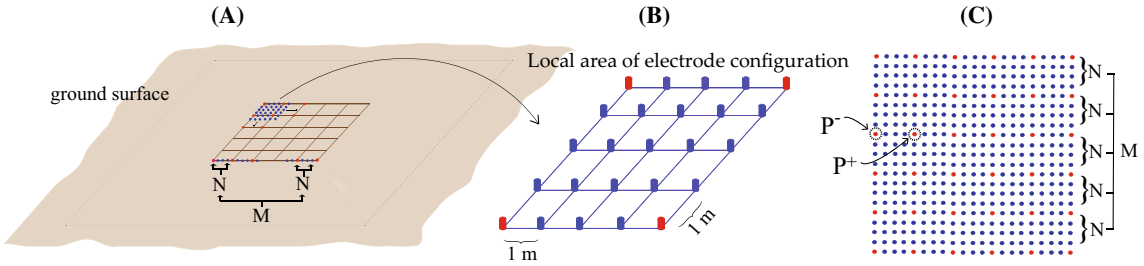

Fig. 1 **a** Electrode configuration on the ground. **b** Magnified local region. **c** Full structure: *red* electrodes are for current injection/voltage measuring, and *blue* electrodes are for voltage measuring only (Color figure online)

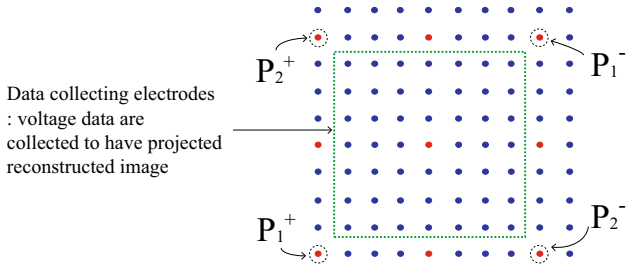

Fig. 2 Projective conductivity imaging method: electrode configuration

the solutions of Eq. (1) corresponding to the injection current, the measured data provide two linearly independent boundary data corresponding to the two artificial injection currents generated by the two pairs of electrodes positioned at $P_1^{\pm}$ and $P_2^{\pm}$, respectively, where $P_1^+ = (0,0)$, $P_1^- = (2N,2N)$, $P_2^+ = (0,2N)$, and $P_2^- = (2N,0)$.

We denote these two corresponding collected data by $V_{i,j}^1$ and $V_{i,j}^2$ at (i,j) for $i,j = 1,\ldots,2N-1$. The projected image reconstruction method is based on Ohm's law projected on the surface. The formula is

$$-\left[\Delta\mathcal{P}_{i,j}\sigma\right]_{t_0}^{t} = \nabla\cdot\left(\left(\begin{array}{cc} V_{i+1,j}^1 - V_{i,j}^1 & V_{i,j+1}^1 - V_{i,j}^1 \\ V_{i+1,j}^2 - V_{i,j}^2 & V_{i,j+1}^2 - V_{i,j}^2 \end{array}\right)^{-1}_{\text{evaluated at } t_0} \left[\begin{array}{c} \Delta V_{i,j}^1 \\ \Delta V_{i,j}^2 \end{array}\right]_{t_0}^{t}\right), \tag{2}$$

where the discrete Laplacian and discrete divergence are defined as

$$\begin{aligned} \Delta V_{i,j}(t) &:= V_{i-1,j}(t) + V_{i+1,j}(t) + V_{i,j-1}(t) \\ &\quad + V_{i,j+1}(t) - 4V_{i,j}(t) \\ \nabla\cdot[\,\alpha_{i,j}(t),\beta_{i,j}(t)\,]^T &:= \alpha_{i+1,j}(t) - \alpha_{i,j}(t) \\ &\quad + \beta_{i,j+1}(t) - \beta_{i,j}(t), \end{aligned}$$

respectively, with the square bracket $[f]_{t_0}^t := f(t) - f(t_0)$. Here $\mathcal{P}_{i,j}\sigma$ represents the relative time change in the conductivity distribution, $(\sigma(t) - \sigma(t_0))/\sigma(t_0)$, at (i,j) in the area of interest, which is projected onto the sensing surface.

In the same manner, this process is repeated by choosing local regions as shown in Fig. 3. Once $\mathcal{P}_{i,j}\sigma$ is obtained by solving (2) on each local region, one can inspect the near-surface underground conductivity distribution locally as well as for the whole area by averaging them and generating the reconstructed image of projected values of σ on the entire target surface.

3 Numerical Simulations

In monitoring underground contamination, two main aspects are continuously surveyed. Conventional EIT is used to generate low-resolution three-dimensional reconstructed images of deep underground, and the projective conductivity image method is used to provide information of the conductivity distribution near the surface.

Conventional EIT utilizes electrodes at positions (iN, jN), $i,j = 0,\ldots,M$ for both driving and sensing. Corresponding to each injected current, the boundary voltage data at time t and position (i,j), other than current-carrying electrodes, are collected and used to visualize the three-dimensional conductivity distribution of the target area. These collected data are also used to generate the projective conductivity image of the local areas.

In the following numerical simulations, we present both cross-sectional images obtained from conventional EIT and projected conductivity images obtained from the projective conductivity image method. Image production is quick in both cases, usually less than seconds.

The computational domain is a square cuboid container of size $40\times40\times30$ m^3. The background soil conductivity is fixed as 1 mS/m, and there are two objects in the underground space with conductivities different from the background (see Fig. 4; Table 1). One is a cylinder of 1 m fixed height at a distance of 8 m from the surface; its radius is set to grow with time. The other object is a tube set to move into the monitoring region 4 m below the surface. This moving tube

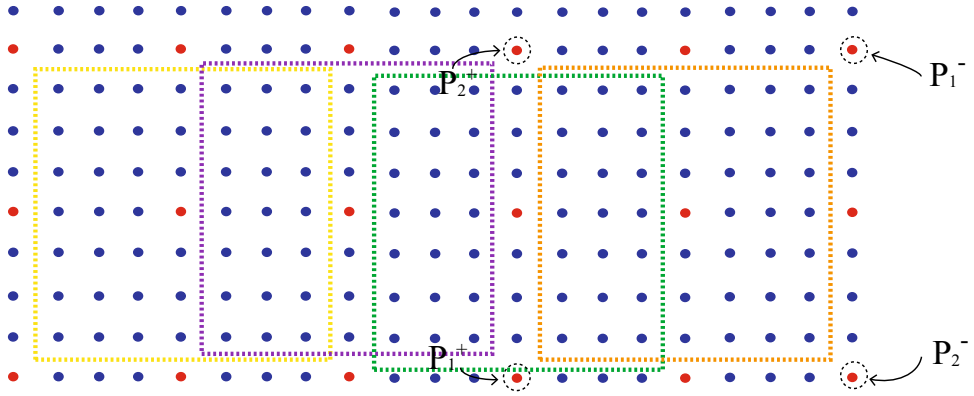

Fig. 3 Projective conductivity imaging method: overall process

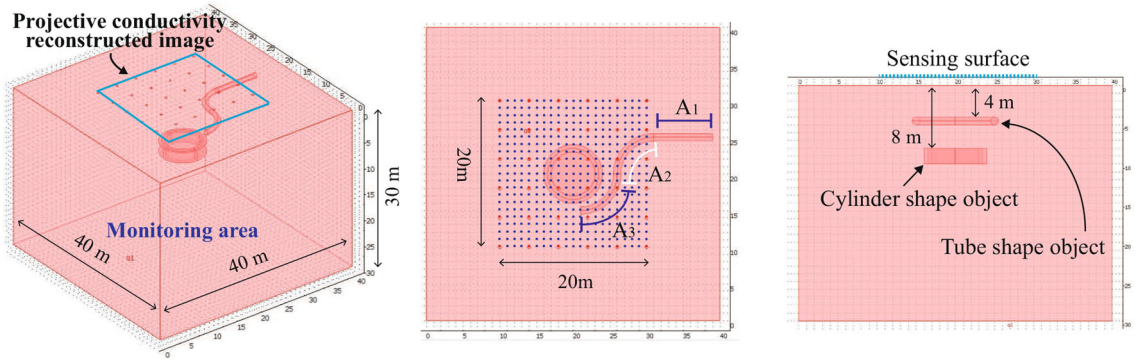

Fig. 4 Computational domain with two moving objects

Table 1 Information of two objects: Object 1 is a radially expanding cylinder, and Object 2 is a moving tube, where A_j, $j = 1, 2, 3$ are from Fig. 4

	Conductivity (mS/m)	At time t_1	At time t_2	At time t_3
Object 1	8	Radius 3 m	Radius 3.5 m	Radius 4 m
Object 2	4	A_1	$A_1 \cup A_2$	$A_1 \cup A_2 \cup A_3$

has a fixed radius of 0.5 m. These objects mimic the time-changing shapes of polluted areas. Table 1 lists their detailed information at three different time s.

First, conventional EIT is used to produce a three-dimensional image of the conductivity distribution underneath the ground surface. It can detect objects far from the sensing surface, but does not provides useful information for the near-surface region owing to the noise that occurs near the electrodes, as shown in Fig. 5. The reconstructed area is $40 \times 40 \times 30$ m^3, and three cross-sectional images are presented in Fig. 5. Figure 5a shows the reconstructed conductivity image for each cross-section using the differences in the voltage data collected at times $t = t_0$ and $t = t_1$. Figure 5b, c are the images obtained by using the differences in the voltage data between $t = t_0$ and $t = t_2, t_3$, respectively. The cross-sectional images at $x = 12$ show little sign of any conductivity changes due to the expanding radius of the cylindrical object, while the images at $x = 20$ clearly show conductivity changes due to the cylindrical object located centrally at 8 m below the surface. In the reconstructed conductivity image at $x = 28$, the entrance of the tubular foreign object is not shown clearly because it is difficult to differentiate from noise in the relatively conductive material.

The projective conductivity image method produces a clear image of the near-surface conductivity distribution. The image of the conductivity distribution in the underground region is projected to the sensing surface, and shown reconstructed as the blue square rectangle area of size 20×20 m^2 in Fig. 4. The top view of the sensing surface is shown in Fig. 6.

A unique feature of the projective conductivity image method is that it provides both local and global conductivity images. If one is interested in particular local areas, for example the square areas in Fig. 6, labeled 'local interested area 1' and 'local interested area 2', then the projective image method can isolate them and reconstruct their projective conductivity images, as shown in Fig. 7.

By patching all the local information, the global projected conductivity distribution can be obtained, as shown in Fig. 8.

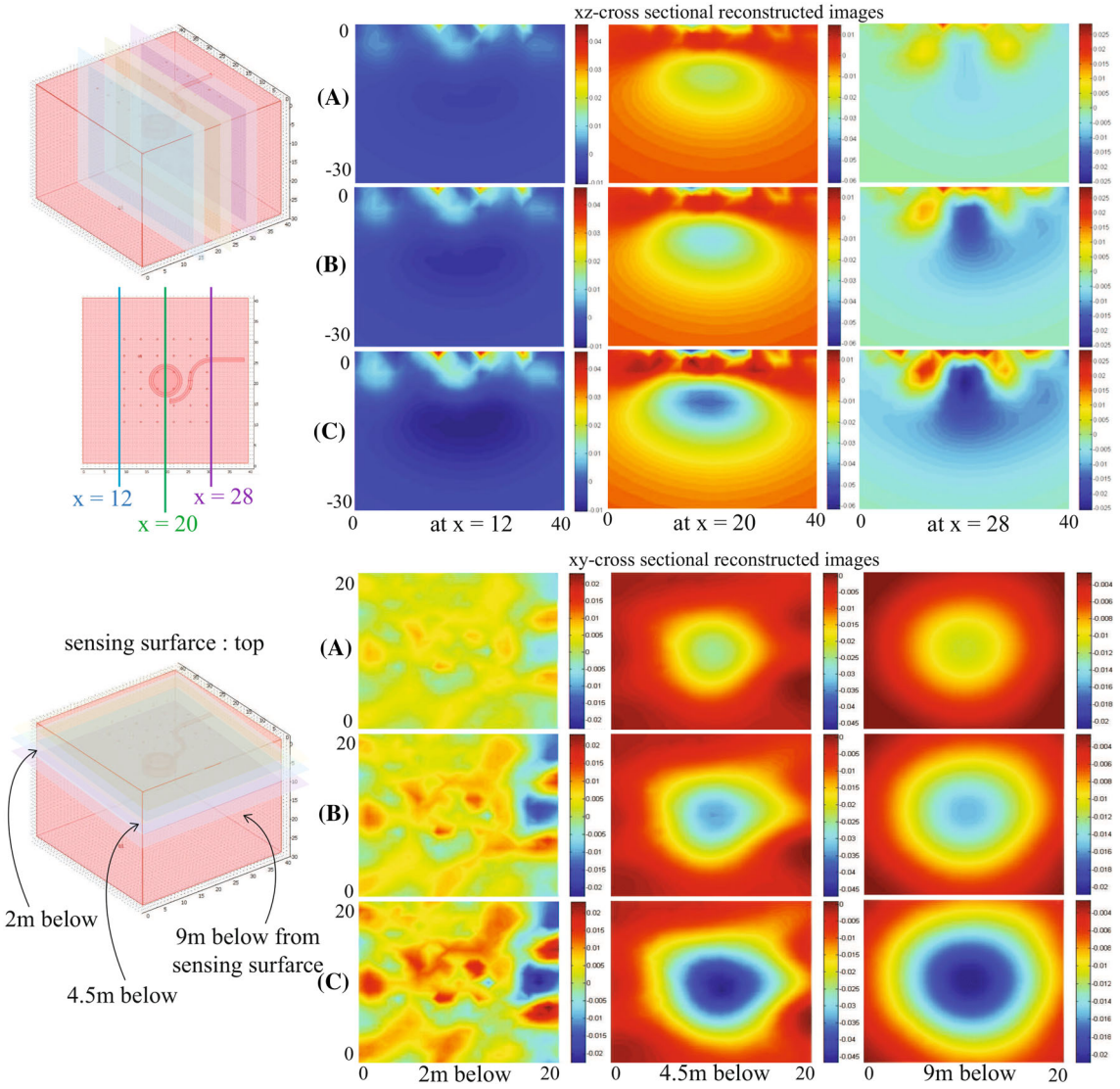

Fig. 5 Reconstructed images of conductivity distribution using conventional EIT: **a** $t = t_1$, **b** $t = t_2$, and **c** $t = t_3$

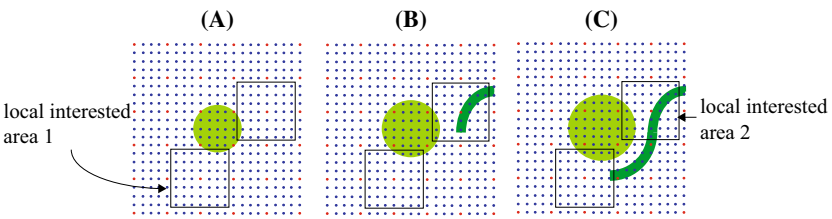

Fig. 6 Top view of the sensing area at each time: **a** $t = t_1$, **b** $t = t_2$, and **c** $t = t_3$

The figure shows that the object in the deeper area is barely detected.

Collecting information through the two different schemes allows the remote real-time monitoring of underground contamination for regions both near to and far from the surface.

4 Phantom Experiments

Phantom experiments are conducted using an agar-filled container with current-injecting/voltage-measuring electrodes fixed at 3.5 cm intervals onto a paper surface. The diameter of each electrode is 1 cm. The electrodes are placed on

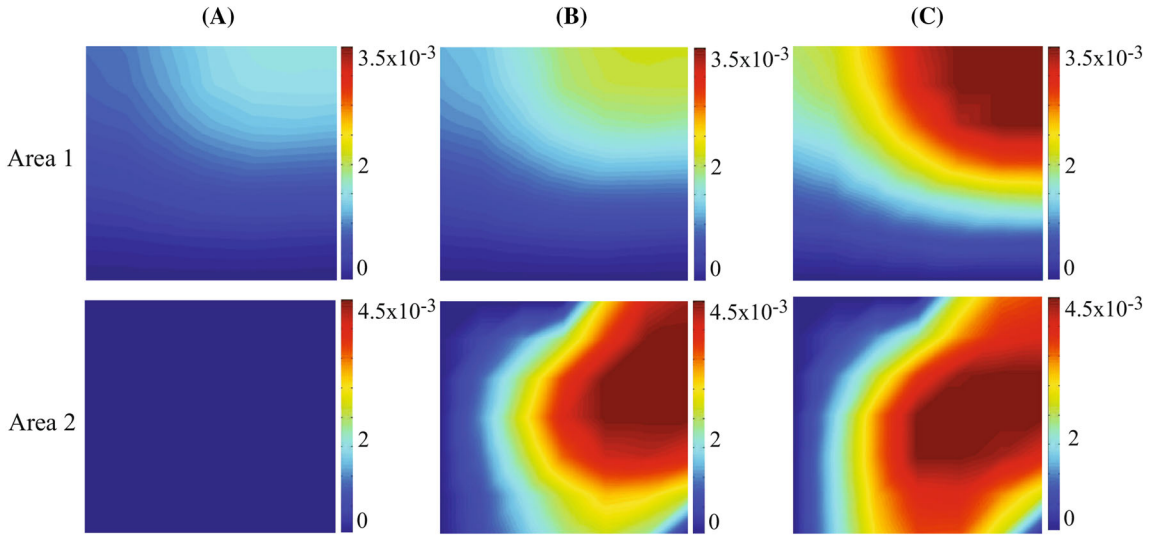

Fig. 7 Local images for the areas in Fig. 6 using the projective method with the difference data: **a** from (t_0, t_1), **b** from (t_0, t_2), and **c** from (t_0, t_3)

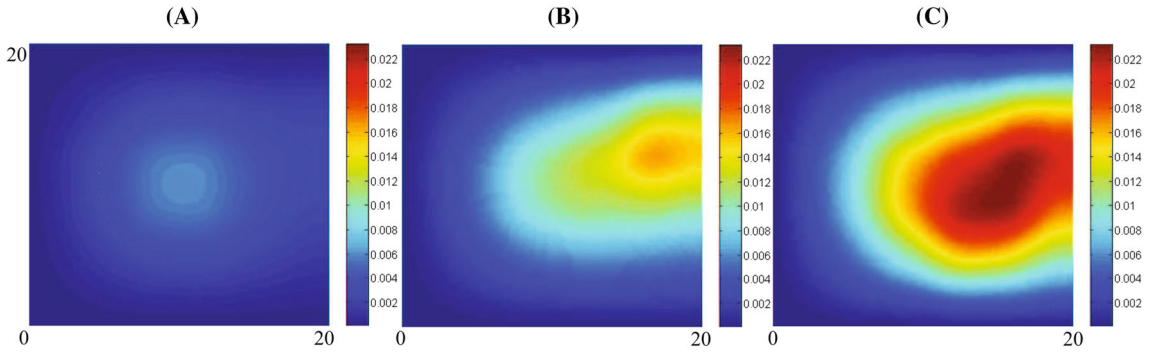

Fig. 8 Reconstructed projective conductivity image of the entire sensing surface using the projective method: **a** from (t_0, t_1), **b** from (t_0, t_2), and **c** from (t_0, t_3)

the surface of the agar such that they are submerged in it (see Figs. 9, 12). A 32-channel Swisstom system ('EIT Pioneer Set') is used to inject the current and to collect the voltage data for reconstructing the conductivity images.

4.1 Reconstructed Conductivity Images Using Conventional EIT

The $28 \times 40 \times 10$ cm^3 container is filled with agar of conductivity 0.143 S/m. A 10 mA current is injected at a frequency of 100 kHz (Fig. 9). The 32 current-injection and voltage-measurement electrodes are placed on top of the agar. The total number of 32×29 voltage data are used to reconstruct the conductivity distribution of the interior of the agar. To lessen the effect of contact impedance, three sets of voltage data are discarded: i.e., those obtained from the current-injecting electrodes and the neighboring electrodes.

Reference voltages are first measured when the container is filled with only agar. Then metal bars of 1.0×10^7 S/m conductivity, 0.7 cm diameter, and varying length (10, 15, and 20 cm) are placed in the agar below and parallel to the sensing surface and 5 cm from the electrode array.

The corresponding sets of voltage data are collected for each bar. The 2D reconstructed images are shown in Fig. 10.

Figure 11 includes the 2D reconstructed image with a hard rubber object of conductivity 1.0×10^{-14} S/m and diameter 1.5 cm placed 5 cm beneath the electrode array.

4.2 Conventional EIT and the Projective Conductivity Image Method Using Two Injection Currents

We compare the reconstructed images obtained from conventional EIT with the ones from the projective conductivity image method. The container is now filled with agar of conductivity 0.2435 S/m, and a current of 10 mA is injected at a frequency of 150 kHz, using the Swisstom system. Due to the unique configuration of the projective conductivity image method, the Swisstom system cannot fully illustrate all of the reconstructed local images mentioned in Sect. 2.2. Accordingly, we conduct phantom experiments with fewer excitation

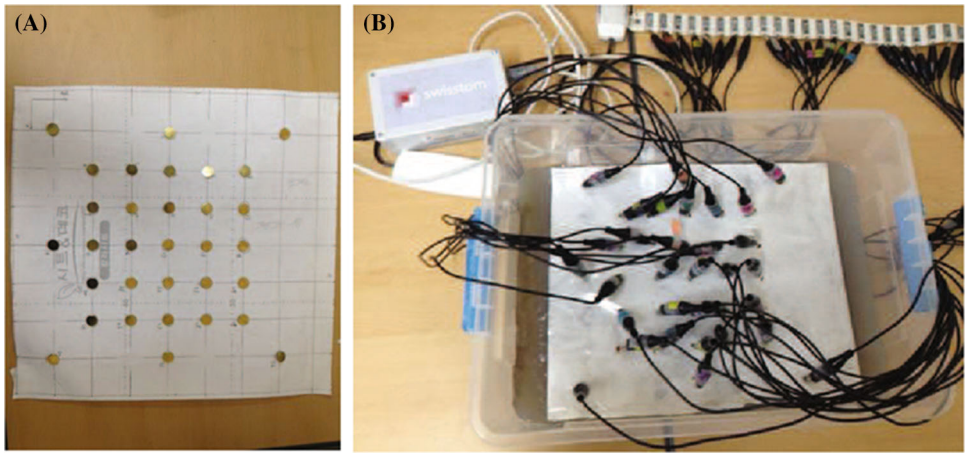

Fig. 9 **a** Electrode array and **b** Swisstom system and experimental setting

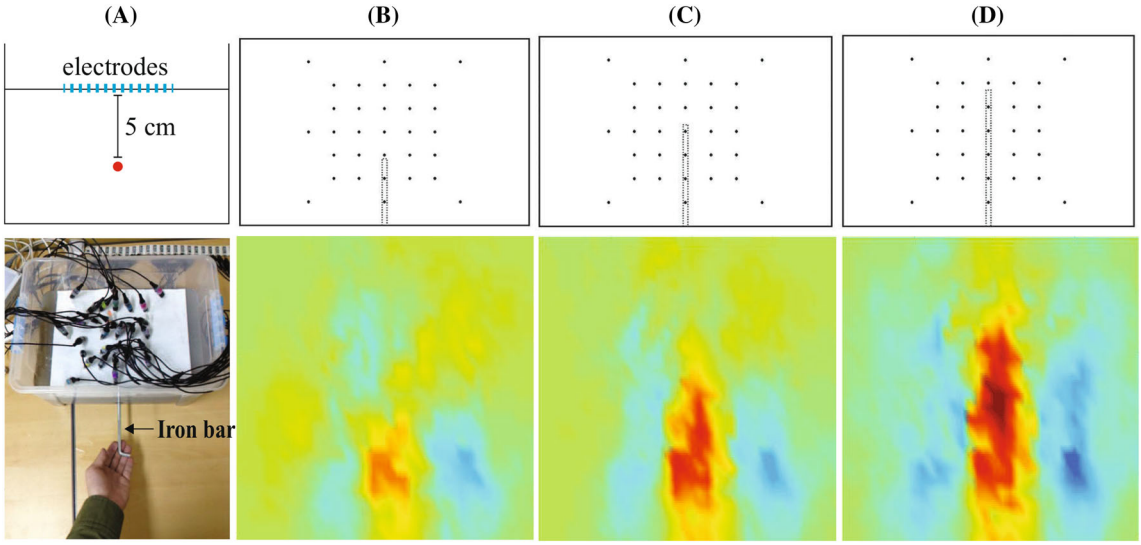

Fig. 10 **a** An iron bar in the container and **b–d** 2D reconstructed images using the Swisstom system with metal bars of length 10, 15, and 20 cm

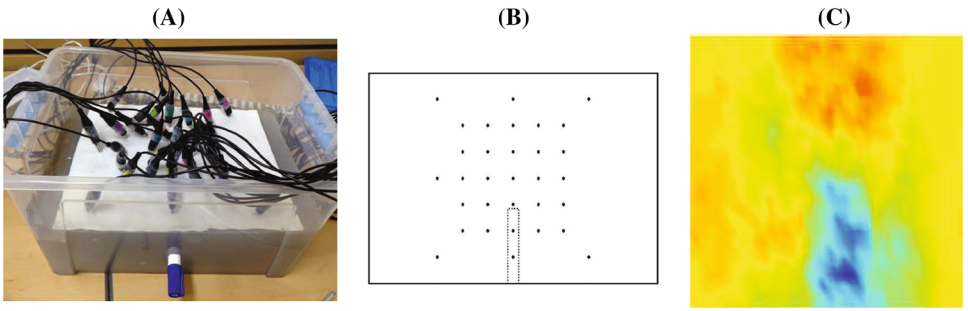

Fig. 11 **a** Experimental setting, **b** top view of the position of the rubber bar, and **c** 2D reconstructed image using Swisstom

patterns of the injected current, as shown in Figs. 12 and 13. The reconstructed images obtained from both conventional EIT and the local projective conductivity image method are given in Fig. 14.

As shown in Fig. 14, the projective conductivity method provides credible information of near-surface conductivity changes with only two injection currents. However, lack of voltage data easily yields poor reconstructed conductivity images with conventional EIT. These results arise from the fundamental difference in the algorithm structures of the two methods. Here we emphasize that, with the proper number of voltage data, conventional EIT can produce conductivity images of a wider and deeper area, but the projective conductivity image method can provide high-resolution local near-surface conductivity images with only two injection currents.

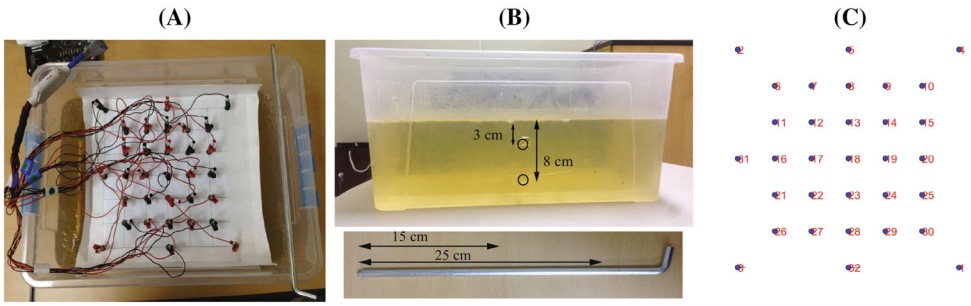

Fig. 12 **a** Top-view photograph of the electrodes, **b** the container and metal bar, and **c** diagram of the electrode array

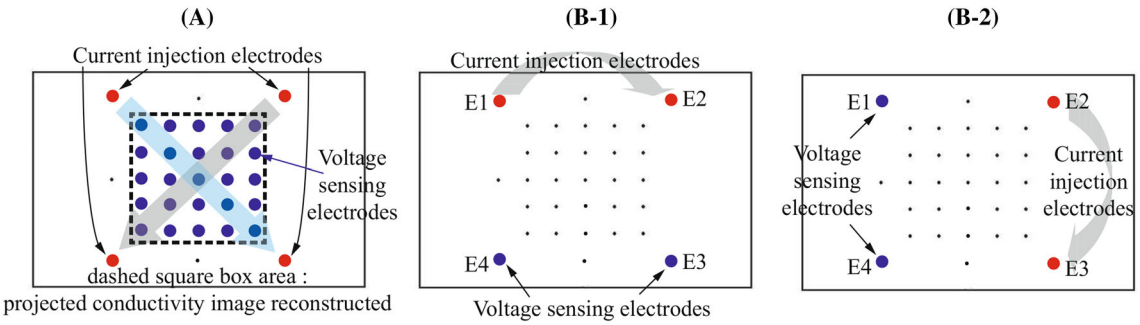

Fig. 13 **a** Electrode configuration for the projective conductivity image method, and **b** conventional EIT: **b-1** when a current is injected through E1 and E2, the voltage data are collected from E3 and E4; analogously, **b-2** when a current is injected through E2 and E3, the voltage is measured at E4 and E1; and current injected through E3 and E4 → voltage measured at E1 and E2

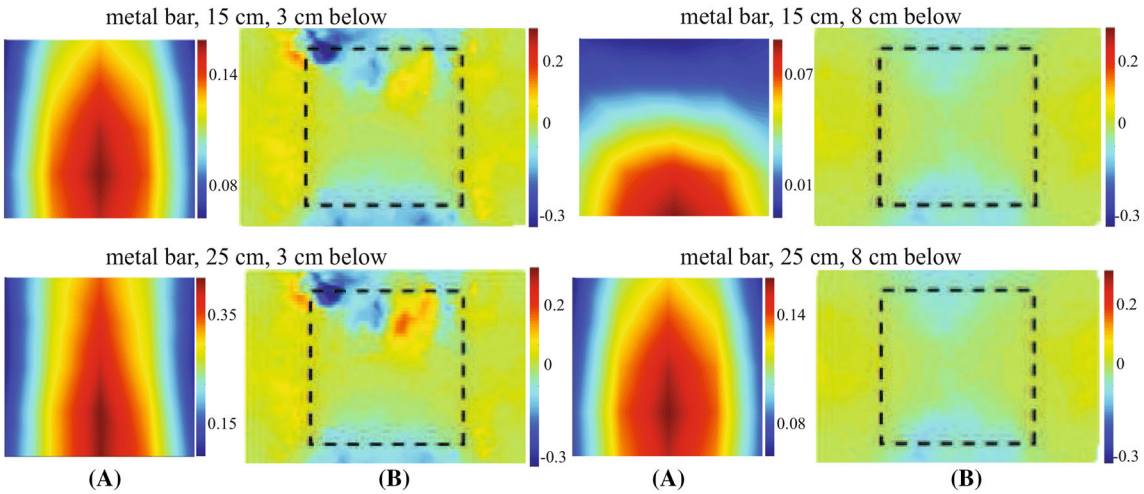

Fig. 14 Reconstructed conductivity images using **a** the projective image method, and **b** conventional EIT (cross-sectional images at 3 and 8 cm below the surface)

5 Conclusion

In this paper, an EIT system is demonstrated for the detection and continuous monitoring of underground contamination. Its installation and maintenance costs are low, and data can be transmitted via various communication methods to enable remote monitoring. The unique EIT electrode configuration introduced here enables the collected voltage data to be used for conventional EIT and the projective conductivity image method. Performing the algorithms for both methods takes less than seconds once the data are collected. Numerical simulations and phantom experiments show that conventional EIT reconstructs the three-dimensional conductivity distribution beneath the sensing ground surface and that the projective conductivity image method successfully produces supplementary local conductivity information of the near-surface underground area. As expected, the projective conductivity image method yields a high-resolution recon-

structed conductivity image of the local near-surface area, but fails to generate the valid information at great depth that conventional EIT can provide. These promising numerical simulation and phantom experiment results can be used to aid the next step of real experiments. Future work will require the construction and installation of the new EIT system shown in Sect. 2.1. We believe that the proposed method will be applicable not only in Mongolia but also to any area that requires continuous monitoring over long time periods.

Acknowledgments This work is supported by NRF Grant 2015 R1A5A1009350.

References

1. Barber, D.C., Brown, B.H.: Applied potential tomography. J. Phys. Sci. Instrum. **17**, 723–733 (1984)
2. Cheney, M., Isaacson, D., Newell, J.C.: Electrical impedance tomography. SIAM Rev. **41**, 85–101 (1999)
3. Clay, R.B.: Conductivity survey: a survival manual. In: Johnson, J.K. (ed.) Remote Sensing in Archaeology: An Explicitly North American Perspective, pp. 80–107. University of Alabama Press, Tuscaloosa (2006)
4. D'Antona, G., Rocca, L.: Electrical impedance tomography for underground pollutant detection and polluted lands reclaiming monitoring. In: IEEE Instrumentation and Measurement Technology Conference Anchorage, AK, USA, 21–23 May 2002
5. Grellier, S., Guerin, R., Robain, H., Bobachev, A., Vermeersch, F., Tabbagh, A.: Monitoring of leachate recirculation in a bioreactor landfill by 2-D electrical resistivity imaging. J. Environ. Eng. Geophys. **13**(4), 351–360 (2008)
6. Hanke, M., Harrach, B., Hyvönen, N.: Justification of point electrode models in electrical impedance tomography. Math. Models Methods Appl. Sci. **21**, 1395–1413 (2011)
7. Metherall, P., Barber, D.C., Smallwood, R.H., Brown, B.H.: Three-dimensional electrical impedance tomography. Nature **380**, 509–512 (1996)
8. Mining in Mongolia: http://en.wikipedia.org/wiki/Mining_in_Mongolia. Accessed 22 Nov 2014
9. Ramirez, A., Daily, W., LaBreque, D., Owen, E., Chesnut, D.: Monitoring an underground steam injection process using electrical resistance tomography. Water Resour. Res. **29**, 73–77 (1993)
10. *Reports of the UN experts' mission to Khongor sum, Darkhan-Uul aming*. http://bic.iwlearn.org/en. Accessed 15 Aug 2008
11. Seo, J.K., Woo, E.J.: Nonlinear Inverse Problems in Imaging. Wiley Press (2012)
12. Ts, M.-E., Lee, E., Seo, J.K., Harrach, B., Kim, S.: Projective electrical impedance reconstruction with two measurements. SIAM J. Appl. Math. **73**(4), 1659–1675 (2013)
13. Tsourlos, P., Ogilvy, R.D., Meldrum, P.I., Williams, G.M.: Time-lapse monitoring in single boreholes using electrical resistivity tomography. J. Environ. Eng. Geophys. **8**(1), 1–14 (2003)
14. Waxman, M.H., Smits, J.M.: Electrical conductivities in oil-bearing shaly sand. Soc. Pet. Eng. J. **243**, 107–122 (1968)
15. Webster, J.: Electrical Impedance Tomography. Adam Hilger, Bristol (1990)
16. Wilkinson, P.B., Meldrum, P.I., Kuras, O., Chambers, J.E., Holyoake, S.J., Ogilvy, R.D.: High-resolution electrical resistivity tomography monitoring of a tracer test in a confined aquifer. J. Appl. Geophys. **70**(4), 268–276 (2010)